HHS Public Access

Author manuscript

Mikrochim Acta. Author manuscript; available in PMC 2023 April 07.

Published in final edited form as:

Mikrochim Acta. ; 189(5): 204. doi:10.1007/s00604-022-05303-8.

3D Printed Microfluidic Device for Automated, Pressure-driven, Valve-injected Microchip Electrophoresis of Preterm Birth Biomarkers

Joule E. Esene[†], **Mawla Boaks**[‡], **Anna V. Bickham**[†], **Gregory P. Nordin**[‡], **Adam T. Woolley**[*,†]

[†]Department of Chemistry and Biochemistry, Brigham Young University, Provo, UT, 84602, USA

[‡]Department of Electrical and Computer Engineering, Brigham Young University, Provo, UT, 84602, USA

Abstract

We developed a 3D printed, automated, pressure-driven injection microfluidic system for microchip electrophoresis (μCE) of preterm birth (PTB)-related peptides and proteins. Functional microvalves were formed, either with a membrane thickness of 5 μm and a layer exposure time of 450 ms, or with a membrane thickness of 10 μm and layer exposure times of 300–350 ms. These valves allowed for control of fluid flow in device microchannels during sample injection for μCE separation. We optimized device design and μCE conditions using fluorescently labeled amino acids. A sample injection time of 0.5 s and a separation voltage of 450 V (460 V/cm) yielded the best separation efficiency and resolution. We demonstrated the first μCE separation with pressure-driven injection in a 3D printed microfluidic device using fluorescently labeled PTB biomarkers and 532 nm laser excitation. Detection limits for two PTB biomarkers, peptide 1 and peptide 2, for an injection time of 1.5 s were 400 pM and 15 nM, respectively, and the linear detection range for peptide 2 was 50–400 nM. This 3D printed microfluidic system holds promise for future integration of on-chip sample preparation processes with μCE, offering promising possibilities for PTB risk assessment.

Graphical abstract

[*]Corresponding author: atw@byu.edu.

Supplementary Information

Supplementary information is available online

Conflict of Interest

A.V.B., G.P.N. and A.T.W. all own shares in Acrea 3D, a company that is commercializing 3D printing of microfluidics.

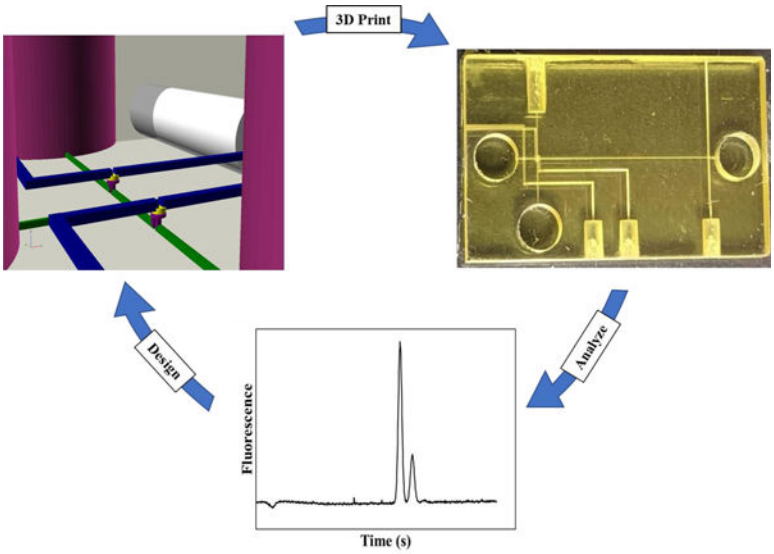

3D printed microfluidic devices with integrated pneumatic valves improve microchip electrophoresis separation biomarkers related to preterm birth risk.

Keywords

3D printing; Microfluidics; Miniaturization; Point of Care; Separations

INTRODUCTION

Microfluidics, the control and manipulation of sub-microliter volumes of fluids in miniaturized device structures [1], finds practical applications in processes that use small fluid volumes to achieve high-throughput analysis [2, 3], multiplexing [4], and automation [5]. Microfluidic devices offer numerous advantages [1]; for example, valves, pumps and channels can be produced to scale in a single device for fluid control [6] and sample preparation processes [7, 8]. These microfluidic systems enable automated multiplexed sample analysis [9] and lower limits of detection (LODs) [7]. Conventional 2D microfabrication methods such as soft lithography [10] and polymer micromachining [11] allow for either prototyping or mass-production of devices. However, conventional 2D microfabrication methods have limitations in fabrication times [12] for creating complex, compact microfluidic features with stacked 2D-planar integrated microfluidic devices [13]. To address these problems, alternative microfluidic device fabrication methods for bioanalysis are needed.

3D printing, an additive manufacturing technology, involves the creation of three-dimensional objects from computer file designs [14]. In recent years, 3D printing has become a useful tool for fabricating miniaturized analytical devices due to advantages of making sophisticated 3D features, not requiring a cleanroom facility, and faster fabrication times [14, 15]. Researchers have reported various analytical advances using 3D printing technology, including histidine-tagged proteins [16], Fe^{2+} [17], blood components [18],

endothelial cells [6], nitric oxide [19], biomarkers [20], and metabolites [21]. Common 3D printing methods have strengths and weaknesses. For example, fused deposition modeling, an extrusion-based 3D printing method, is easy to use and inexpensive but is typically limited to fluidic structures larger than ~1 mm in cross section, although recent customized nozzles have lowered that limit [22]. Polyjet 3D printing can use a broader range of polymers with multiple materials in a single device, but sacrificial layers limit channel sizes [23]. Stereolithography (SL) avoids the use of sacrificial materials, but generally only creates devices from a single polymer. Typical SL prints can have fluidic features nearing the 100 μm range [24], but this still leaves important microfluidic applications such as microchip electrophoresis (μCE) inaccessible. To overcome limitations of current 3D printing methods, the Woolley and Nordin groups developed a high-resolution SL 3D printer that can print fluidic features as small as 20 μm x 20 μm [25]. This 3D printer allows rapid and scalable fabrication of complex integrated microfluidic systems, including fluidic interconnects [26], as well as pumps and valves [27]. These enhanced capabilities make this 3D printer an excellent option for the fabrication of integrated microfluidic systems for bioanalysis.

Microchip electrophoresis is a method that takes advantage of miniaturization in microfluidics [28, 29]. The simplest approach for μCE employs electrokinetic injection [30], which has seen widespread use. Pressure-regulated injection is a less common alternative, which allows sampling from flowing solutions [31], combination with sample preparation [7, 32], or working with samples that have low or high ionic strength [7, 32].

Preterm birth (PTB) follows labor that occurs before 37 weeks of pregnancy; it is the principal cause of neonatal mortality, with about 1 million deaths recorded globally in 2015 due to preterm complications [33]. Unfortunately, clinical determination of risk for PTB remains a critical need. A panel of nine maternal serum biomarkers has been initially evaluated and shown to have ~90% sensitivity and >80% specificity in predicting PTB risk up to four weeks before contractions [34, 35]. Conventional analytical methods, though effective for finding PTB biomarkers, have limitations for rapid analysis. For example, liquid chromatography-mass spectrometry of PTB peptides is complicated by personnel-intensive sample preparation steps [34], and enzyme-linked immunosorbent assay is not well suited for multiplexing proteins and peptides [36, 37]. Consequently, the need for better analysis methods for PTB biomarkers is crucial. Our group focuses on developing integrated microfluidics for PTB biomarker analysis [7, 38, 39], which requires miniaturized fluid handling to effectively combine on-chip sample preparation steps with analysis. Integrating upstream sample preparation processes with separations is a crucial step for analyzing samples in a real biofluid matrix, as this can improve LODs and μCE performance. Importantly, 3D printing offers a promising strategy for creating microdevices that integrate sample preparation with μCE to carry out PTB biomarker analysis.

Here, we show 3D printing of microfluidic devices for the first time to allow valve-injected electrophoretic separation of PTB biomarkers. Characterization of valves and optimization of sample injection times were performed. We obtained good separation efficiency and resolution with 3D printed valve-injected microfluidic devices by automated control of sample injection time. We further demonstrated the separation of fluorescently labeled

PTB biomarkers in these devices. Such valve-integrated microdevices are crucial to future combination of upstream sample preparation processes with μCE separation in a single system for PTB biomarker analysis.

MATERIALS AND METHODS

Materials.

Polyethylene glycol diacrylate (PEGDA, 258 Da MW), phenylbis (2,4,6-trimethylbenzoyl)-phosphine oxide (Irgacure 819), 3-(trimethoxysilyl)propyl methacrylate, hydroxypropyl cellulose (HPC, 300 kDa), 4-(2-hydroxyethyl)-1-piperazineethanesulfonic acid (HEPES), and dimethyl sulfoxide (DMSO) were purchased from Sigma-Aldrich (Milwaukee, WI). 2-Nitrodiphenylsulfide (NPS) was from TCI America (Portland, OR). AlexaFluor 532 NHS ester (AF), acetone, and 2-propanol (IPA) were purchased from Fisher Scientific (Salt Lake City, UT). Glycine (G), ferritin (Fer), hydrochloric acid, sodium carbonate, and Amicon ultra 0.5 mL centrifuge filters were from Millipore Sigma (Billerica, MA). Sodium hydroxide was acquired from Mallinckrodt Specialty Chemicals (St. Louis, MO). Sodium bicarbonate monobasic was purchased from Merck (Burlington, MA). Toluene and glass microscope slides (3 × 1 in, 1 mm thick) were from Avantor (Center Valley, PA). Phenylalanine (F) was obtained from Spectrum Chemical (New Brunswick, NJ). PTB Peptide 1 (P1) and PTB Peptide 2 (P2) [39] were acquired from Biomatik (Wilmington, DE). Corticotropin releasing factor (CRF) was purchased from GeneScript (Piscataway, NJ). Lactoferrin (LF) was from Sigma (St. Louis, MO). Water purified to 18.3 MΩ·cm by a Barnstead EASYpure UV/UF system (Dubuque, IA) was used to prepare all solutions.

Device fabrication.

Valve-integrated microfluidic devices were designed using OpenSCAD (openscad.org) as shown in Figure 1a. The layout of the electrophoretic separation system is adapted from our prior work [38]. The design comprised a six-pixel wide (46 μm) by five-layer deep (50 μm) injection channel connected to two integrated pneumatic valves of 20 pixel (152 μm) diameter for fluid control, a vacuum line for sample flow during injection, and one 2.7 mm diameter × 0.75 mm deep fluid reservoir. The design also had a 9.8 mm long, six-pixel wide (46 μm) by five-layer tall (50 μm) separation channel connected to two pneumatic valves and reservoirs. Zoom views of valve positions in the device layout are given in Figure 1b–c.

Microfluidic devices were 3D printed using a custom-built SL 3D printer, as in a previous paper [38]. In summary, the resin formulation comprised 97% PEGDA (monomer), 2% NPS (UV absorber), and 1% Irgacure 819 (photoinitiator), and was introduced into the 3D printer resin tray. Next, a glass slide treated with 3-(trimethoxysilyl)propyl methacrylate and stored in toluene was attached to the 3D printer build platform to serve as the support for the 3D print. Finally, the OpenSCAD design was electronically sent to the 3D printer for printing, and post-cure exposure of the 3D print was done afterwards. The layer exposure time in the bulk material was 1000 ms, modified to 400 ms for two pixels surrounding the injection and separation channels. Valves with membrane thicknesses of 5 and 10 μm were 3D printed with layer exposure times of 300–450 ms for testing.

Sample preparation.

Buffer for samples was prepared using sodium bicarbonate and sodium carbonate (10 mM BCB), adjusted to pH 10 using sodium hydroxide. 2 mM AF solution for fluorescent labeling of samples was prepared by dissolving AF in DMSO. Next, 1 mM G was prepared by dissolving 7.5 mg in 100 μL of BCB and diluting to 1 mM with BCB, 1 mM F was made by dissolving 1.65 mg in 1 mL of BCB and diluting to 1 mM in BCB, 0.5 mM P1 was prepared by dissolving 0.1 mg of P1 in 100 μL of BCB, 0.2 mM CRF was generated by dissolving 1 mg of CRF in 1 mL of BCB, and 0.06 mM LF was made by dissolving 5 mg of LF in 1 mL of BCB. All these molecules were fluorescently labeled with 2 mM AF, and incubated in the dark at room temperature for at least 12 hrs. The molar labeling ratio for G and F was 10/1 sample/AF. The molar labeling ratios for P1, CRF, and LF were 1/1, 2/3, and 1/15 sample/AF, respectively. LF solution was filtered with a 30 kDa cut-off filter to remove excess dye. 0.5 mM P2 prepared by dissolving 2.1 mg of P2 in 1 mL of BCB and 10 μM Fer prepared by dissolving 5 mg of Fer in 1 mL of BCB were both fluorescently labeled with 2 mM AF, and incubated in the dark at a temperature of 40 °C for at least 12 hrs. The molar labeling ratios for P2 and Fer were 1/10 and 1/30 sample/AF, respectively. After incubation, fluorescently labeled P2 and Fer solutions were filtered with 3 kDa or 50 kDa cut-off filters (4×, 14 000 rpm, 15 min), respectively, to remove excess dye. Finally, labeled samples were diluted to working concentrations in the nM range in 10 mM BCB (pH 10); analyte concentrations for specific experiments are given in Figure captions. P1 and P2 concentrations were selected to allow LODs to be determined in our system, as the clinically relevant levels in serum have yet to be determined.

Device testing.

After 3D printing valve-integrated microfluidic devices, the performance of the valves was tested by first closing valves controlling fluid flow to the separation channel (Figure S1a) while leaving valves connected to the injection channel open. Next, fluorescent dye was pulled with vacuum into the injection intersection. Injection valve leakage testing was performed using 532 nm laser excitation with a Hamamatsu ORCA-Fusion CMOS camera (Bridgewater, NJ) to monitor flow of fluorescent dye into the separation channel. In an additional experiment, both valves 2 were closed, vacuum was turned on, and the injection intersection was observed for flow of fluorescent dye. Valve tests were performed with pressures between 25–45 psi. To further investigate the integrity of the valves, a point detection experiment was performed, wherein fluorescent dye was flowed into the injection channel (valves 2 open), and fluorescence was recorded in the separation channel (Figure S1a) using a Hamamatsu photomultiplier tube (PMT, Bridgewater, NJ).

μCE separation.

Once the valves were confirmed to be functional, μCE experiments were performed to test the separation performance of the microfluidic device using fluorescently labeled solutions of G and F. For μCE experiments, 50 mM HEPES, pH 8, with 1% HPC (w/w) served as the running buffer. The μCE setup consisted of a valve system that was automated through control software and a laser induced fluorescence (LIF) detection system. The LIF detection system had a 532 nm laser (4 mW, Laserglow Technologies, Toronto, ON) that

went through a dichroic mirror (Semrock, Rochester, NY) and entered an Axio Observer.A1 inverted microscope (Zeiss, Jena, Germany) with a Chroma ET-532 nm laser band and long pass filter set (Rockingham, VT). A 20 × objective lens focused the excitation source within the channel and collected fluorescent photons. Voltage was controlled using a high-voltage power supply (PS350, Stanford Research Systems, Sunnyvale, CA) and a custom voltage switching box, which was connected to the device using platinum electrodes. Fluorescence was detected at a Hamamatsu PMT. The analog PMT output was processed using a preamplifier (SR-560, Stanford Research Systems), digitized with a NI USB-6212 analog-to-digital converter (National Instruments, Austin, TX) and recorded at 20 Hz using LabVIEW software (National Instruments). Fluorescence was measured 1.0 mm from the end of the separation channel. The valve system used PTFE tubing (0.022 in ID × 0.042 in OD; Cole Parmer, Vernon Hills, IL) which was inserted into the openings on the side of the device (Figure 1) to facilitate pressure and vacuum connection. First, all valves were closed by pressure actuation (40 psi), and 6 μL of running buffer was filled into reservoirs 1 and 3 (Figure S1). Next, 5.5 μL of a mixture of 80 nM G and 120 nM F was filled into reservoir 2. Following that, platinum electrodes were connected to reservoirs 1 and 3, and the voltage (450 V) and vacuum were switched on. Then, the valve 2 set was opened, and sample was flowed through the injection intersection for 0.1–2.0 s, with the injection duration given by the time between opening and closing the valve 2 set (Figure S1a). Immediately as the valve 2 set was closed, valves 1 and 3 were opened to apply the voltage for μCE separation to be carried out (Figure S1b). Similarly, μCE experiments were performed for PTB biomarkers with an injection time of 0.5 s and a separation voltage of 450 V.

RESULTS AND DISCUSSION

Figure 1d shows a photograph of a 3D printed valve-integrated device. Microchannels can be seen running between an opening on the side of the device and the sample reservoir, as well as between the high voltage and ground reservoirs. Three pneumatic lines are connected to openings on one side of the device. The device has a total of four valves, with valves 1 and 3 controlling fluid flow in the separation channel, and the valve 2 set controlling fluid flow in the injection channel. The valve 2 set has a spacing of 8 pixels (61 μm), from the edge of the valve to the edge of the separation channel. This spacing allows the formation of a sample plug with an approximate volume of 800 pL.

Initial experiments focused on characterization of the valves [26, 27]. Valves of different membrane thicknesses were designed and 3D printed under varying exposure times. Valves worked reproducibly with a membrane thickness of 5 μm formed with a layer exposure time of 450 ms, as well as with a membrane thickness of 10 μm and created with layer exposure times of 300 or 350 ms. In contrast, valves were not reproducible with a membrane thickness of 5 μm formed with layer exposure times of 300–400 ms, or with a membrane thickness of 10 μm formed with layer exposure times of 400 or 450 ms. The reproducible valves formed without tears, and would open and close, whereas the irreproducible valves formed were broken, or would not open and close. Flow tests were recorded as seen in the Supplementary Information (Movie S1.mp4 and Movie S2.mp4). These experiments showed that the valves only allowed fluid flow through the separation or injection channel when opened, and blocked fluid flow when closed, confirming their functionality. The

magnification and focus in these videos are also sufficient to resolve individual 7.6 μm pixels that look grid-like in some of the 3D printed fluidic features.

In this work, samples were prepared in 10 mM BCB (pH 10), which contained both sodium carbonate and sodium bicarbonate, rather than 10 mM sodium bicarbonate (pH 9.5) [38]. BCB resulted in more stable current during μCE compared to the previously used sodium bicarbonate, likely due to better pH buffering and lower overall current for a given voltage with BCB. We also evaluated injection pressure differentials from 1–10 psi and found that 5.0–7.5 psi provided the most reliable injections across a range of loading times (Table S1), so we chose a pressure differential of 7 psi for further study. Tests on sample injection times between 0.1–2.0 s were performed to determine what time was best suited for electrophoretic separation of G and F using these devices. Figure 2a shows the electropherogram for a sample injection time of 0.5 s. The two dye peaks, and the G and F peaks were all resolved. Figures 2b and c show electropherograms for sample injection times of 1.0 and 1.5 s, respectively. The peak heights obtained for the 0.5 s injection time were comparable to peak heights obtained for similar amino acid concentrations in μCE in our previous work [38]. As seen in Figure 2, peak width broadened and peak height increased modestly as the injection time increased from 0.5–1.5 s. Peak heights for the analytes were either inconsistent or sometimes no peaks were observed when the injection time was reduced below 0.5 s, most likely because not enough time was allowed for sample to be reproducibly loaded into the separation channel intersection. Analyte peaks broadened and had off-scale signal when the injection time was increased above 1.5 s. The separation results, including peak height, FWHM, separation efficiency, and resolution between G and F, were measured, along with their standard deviations, for injection times of 0.5, 1.0, and 1.5 s (Table 1). A plot of number of theoretical plates as a function of injection time in Figure S2 showed that as the injection time increased, the number of theoretical plates decreased. An injection time of 0.5 s yielded the highest separation efficiency and resolution for the analytes. A key advantage of using pneumatic valves for sample injection is the precise introduction of a small-volume sample, providing good separation performance with short injection times.

PTB biomarker separation.

Building on the results from amino acid separations, we used similar conditions to separate multiple PTB biomarkers. Figure 3a shows a microchip electropherogram of P1, P2, CRF, and Fer, with all analytes resolved. Fer, a protein biomarker, had a broader peak than the peptide biomarkers in the electropherogram due to its larger size and number of fluorescent labeling sites, causing a wider distribution of charges after labeling [38, 39]. Encouraged by this result, we added another PTB biomarker (LF), and Figure 3b shows a microchip electropherogram of five PTB biomarkers. Like Fer, LF also had a broad peak due to its molecular weight. The dye peak height varied between the two runs because different samples were injected. Table 2 lists pairs of PTB biomarkers and their resolution values, which range from 1.5–3.1 and are comparable to our previous work in conventional polymer microdevices [39].

We also investigated the LODs for G, P1, and P2 in our microfluidic devices; all samples were analyzed in triplicate at injection times of 0.5, 1.0 and 1.5 s. Figures S3a–c show the calibration plots for G, which had LODs of 15, 9, and 4 nM, respectively. Figure S3d–e and Figure 4 show the calibration plots for P1, which had LODs 700, 600, and 400 pM, respectively. Figures S3f–h show the results for P2, which had LODs 42, 28, and 15 nM, respectively. For all samples, the LODs improved as sample injection time increased from 0.5–1.5 s, consistent with the expectation of higher sample loading with longer injection times. In previous μCE work [39] where electrokinetic injection was employed, LODs for P1 and P2 were 3 nM and 190 nM, respectively; thus, our valve-based, pressure driven injection improved LODs by as much as tenfold. Additionally, the working concentration ranges for G, P1, and P2 were 10–100 nM, 1–5 nM, and 40–450 nM, respectively, and the linear dynamic range for peptide 2 was 50–400 nM. Table 3 provides a summary comparison of our results with prior publications where these PTB biomarkers were also analyzed. Importantly, this represents the first successful demonstration of μCE separation of five PTB biomarkers in a 3D printed microfluidic device, also with the lowest LODs reported to date for these PTB biomarkers. This separation further improves over our previous work [38], where three PTB biomarkers were separated in a 3D printed device with voltage-based injection. This improvement may be due to better sample injection achieved using pneumatic valves for fluid control as opposed to electrokinetic injection. It also demonstrates that good separation efficiency can be achieved with valve-based injection in 3D printed microfluidic devices. Fluid control using on-chip valves may allow integration of upstream sample preparation processes, potentially saving time, providing automation, and improving PTB biomarker LODs. We also note that it may be feasible to improve separation performance by 3D printing serpentine channels [25] with tapered turns. Some future areas for improvement of our methods include optimizing valve membrane robustness under applied voltages, streamlining the processes for creating world-to-chip interconnects, and analysis of human serum samples.

CONCLUSION

We developed valve-integrated microfluidic systems for μCE separation of PTB biomarkers. The valves allowed control of fluid for pressure-driven injection during μCE, eliminating sample injection bias by electrophoretic mobility observed in electrokinetic injection. This work is the first to demonstrate pressure-driven injection with μCE separation in a 3D printed microfluidic device. Additional studies that may be done to overcome challenges of valve membrane wear-and-tear after being subjected to high voltages for a long time involve resin development to improve strength of the device material. Another experiment that may be done is to further optimize layer exposure times in the device.

A key benefit of our 3D printed microfluidics is that they open the door to integration of upstream sample preparation processes, such as immunoaffinity extraction of serum samples [40], and preconcentration and fluorescent labeling [41], with μCE separation. In particular, on-chip preconcentration processes should lower detection limits in μCE [42]. 3D printing also offers a promising path for improving separation performance, for example, by creating serpentine channels with tapered turns. These advances should enable the development of 3D printed microfluidics for PTB biomarker risk assessment. The general applicability of

3D printed integrated microfluidics further offers excellent potential for future developments in the field of bioanalysis.

Supplementary Material

Refer to Web version on PubMed Central for supplementary material.

Acknowledgements

We thank the National Institutes of Health for funding this work (R01 EB027096).

References

[1]. Nielsen JB, Hanson RL, Almughamsi HM, Pang C, Fish TR, Woolley AT (2019) Microfluidics: innovations in materials and their fabrication and functionalization. Anal Chem, 92(1) 150–168. [PubMed: 31721565]

[2]. Urbanska M, Muñoz HE, Shaw BJ, Otto O, Manalis SR, Di Carlo D, Guck J (2020) A comparison of microfluidic methods for high-throughput cell deformability measurements. Nature Methods 17(6), 587–593. [PubMed: 32341544]

[3]. Wang C, Wang C, Qiu J, Gao J, Liu H, Zhang Y, Han L (2021) Ultrasensitive, high-throughput, and rapid simultaneous detection of SARS-CoV-2 antigens and IgG/IgM antibodies within 10 min through an immunoassay biochip. Microchim Acta 188(8), 1–15.

[4]. Dai B, Yin C, Wu J, Li W, Zheng L, Lin F, Zhuang S (2021) A flux-adaptable pump-free microfluidics-based self-contained platform for multiplex cancer biomarker detection. Lab Chip 21(1), 143–153. [PubMed: 33185235]

[5]. Mora MF, Kehl F, Tavares da Costa E, Bramall N, Willis PA (2020) Fully automated microchip electrophoresis analyzer for potential life detection missions. Anal Chem 92(19) 12959–12966. [PubMed: 32842727]

[6]. Castiaux AD, Selemani MA, Ward MA, & Martin RS (2021) Fully 3D printed fluidic devices with integrated valves and pumps for flow injection analysis. Anal Meth 13(42), 5017–5024.

[7]. Sahore V, Sonker M, Nielsen AV, Knob R, Kumar S, Woolley AT (2018). Automated microfluidic devices integrating solid-phase extraction, fluorescent labeling, and microchip electrophoresis for preterm birth biomarker analysis. Anal Bioanal Chem, 410(3) 933–941. [PubMed: 28799040]

[8]. Li F, Guijt RM, Breadmore MC (2016) Nanoporous membranes for microfluidic concentration prior to electrophoretic separation of proteins in urine. Anal Chem 88(16) 8257–8263. [PubMed: 27391148]

[9]. Mitchell KR, Esene JE, Woolley AT (2022) Advances in multiplex electrical and optical detection of biomarkers using microfluidic devices. Anal Bioanal Chem, 414(1) 167–180. [PubMed: 34345949]

[10]. Qin D, Xia Y, Whitesides GM (2010) Soft lithography for micro-and nanoscale patterning. Nature Protocols, 5(3), 491. [PubMed: 20203666]

[11]. Kim BJ, Meng E (2015) Review of polymer MEMS micromachining. J Micromech Microengin 26(1) 013001.

[12]. Walsh III DI, Kong DS, Murthy SK, Carr PA (2017) Enabling microfluidics: from clean rooms to makerspaces. Trends Biotechnol 35(5) 383–392.. [PubMed: 28162773]

[13]. Morbioli GG, Speller NC, Stockton AM (2020) A practical guide to rapid-prototyping of PDMS-based microfluidic devices: a tutorial. Anal Chim Acta 1135 150–174. [PubMed: 33070852]

[14]. Nielsen AV, Beauchamp MJ, Nordin GP, Woolley AT (2020) 3D printed microfluidics. Annu Rev Anal Chem 13 45–65.

[15]. Waheed S, Cabot JM, Macdonald NP, Lewis T, Guijt RM, Paull B, Breadmore MC (2016) 3D printed microfluidic devices: enablers and barriers. Lab Chip 16(11) 1993–2013. [PubMed: 27146365]

[16]. Arshavsky-Graham S, Enders A, Ackerman S, Bahnemann J, Segal E (2021) 3D-printed microfluidics integrated with optical nanostructured porous aptasensors for protein detection. Microchim Acta 188(3) 1–12.

[17]. Balavandy SK, Li F, Macdonald NP, Maya F, Townsend AT, Frederick K, Breadmore MC (2021) Scalable 3D printing method for the manufacture of single-material fluidic devices with integrated filter for point of collection colourimetric analysis. Anal Chim Acta 1151 238101. [PubMed: 33608072]

[18]. Chen C, Wang Y, Lockwood SY, Spence DM (2014) 3D-printed fluidic devices enable quantitative evaluation of blood components in modified storage solutions for use in transfusion medicine. Analyst 139(13) 3219–3226. [PubMed: 24660218]

[19]. Munshi AS, Chen C, Townsend AD, Martin RS (2018) Use of 3D printing and modular microfluidics to integrate cell culture, injections and electrochemical analysis. Anal Meth 10(27) 3364–3374.

[20]. Singh M, Tong Y, Webster K, Cesewski E, Haring AP, Laheri S, Johnson BN (2017) 3D printed conformal microfluidics for isolation and profiling of biomarkers from whole organs. Lab Chip 17(15) 2561–2571. [PubMed: 28632265]

[21]. Gowers SA, Curto VF, Seneci CA, Wang C, Anastasova S, Vadgama P, Boutelle MG (2015) 3D printed microfluidic device with integrated biosensors for online analysis of subcutaneous human microdialysate. Anal Chem 87(15) 7763–7770. [PubMed: 26070023]

[22]. Quero RF, da Silveira GD, da Silva JAF, de Jesus DP (2021) Understanding and improving FDM 3D printing to fabricate high-resolution and optically transparent microfluidic devices. Lab Chip 21(19) 3715–3729. [PubMed: 34355724]

[23]. Castiaux AD, Pinger CW, Hayter EA, Bunn ME, Martin RS, Spence DM (2019) PolyJet 3D-printed enclosed microfluidic channels without photocurable supports. Anal Chem 91(10) 6910–6917. [PubMed: 31035747]

[24]. Gong H, Woolley AT, Nordin GP (2016) High density 3D printed microfluidic valves, pumps, and multiplexers. Lab Chip 16(13) 2450–2458. [PubMed: 27242064]

[25]. Gong H, Bickham BP, Woolley AT, Nordin GP (2017) Custom 3D printer and resin for 18 μm× 20 μm microfluidic flow channels. Lab Chip 17(17) 2899–2909. [PubMed: 28726927]

[26]. Sanchez Noriega JL, Chartrand NA, Valdoz JC, Cribbs CG, Jacobs DA, Poulson D, Nordin GP (2021) Spatially and optically tailored 3D printing for highly miniaturized and integrated microfluidics. Nature Commun 12(1) 5509. [PubMed: 34535656]

[27]. Gong H, Woolley AT, & Nordin GP (2018) 3D printed high density, reversible, chip-to-chip microfluidic interconnects. Lab Chip 18(4) 639–647. [PubMed: 29355276]

[28]. Caruso G, Musso N, Grasso M, Costantino A, Lazzarino G, Tascedda F, Caraci F (2020) Microfluidics as a novel tool for biological and toxicological assays in drug discovery processes: Focus on microchip electrophoresis. Micromachines 11(6) 593. [PubMed: 32549277]

[29]. Chotteau V (2021) Knowing more from less: miniaturization of ligand-binding assays and electrophoresis as new paradigms for at-line monitoring and control of mammalian cell bioprocesses. Curr Opin Biotechnol 71, 55–64. [PubMed: 34246047]

[30]. Harrison DJ, Manz A, Fan Z, Luedi H, Widmer HM (1992) Capillary electrophoresis and sample injection systems integrated on a planar glass chip. Anal Chem 64(17) 1926–1932.

[31]. Drevinskas T, Maruška A, Girdauskas V, Dūda G, Gorbatsova J, Kaljurand M (2020) Complete capillary electrophoresis process on a drone: towards a flying micro-lab. Anal Meth 12(41) 4977–4986.

[32]. Mecker LC, Martin RS (2008) Integration of microdialysis sampling and microchip electrophoresis with electrochemical detection. Anal Chem 80(23) 9257–9264. [PubMed: 19551945]

[33]. Liu L, Oza S, Hogan D, Chu Y, Perin J, Zhu J, Black RE (2016) Global, regional, and national causes of under-5 mortality in 2000–15: an updated systematic analysis with implications for the Sustainable Development Goals. Lancet 388(10063) 3027–3035. [PubMed: 27839855]

[34]. Esplin MS, Merrell K, Goldenberg R, Lai Y, Iams JD, Mercer B, Eunice Kennedy Shriver National Institute of Child Health and Human Development Maternal-Fetal Medicine Units

Network (2011) Proteomic identification of serum peptides predicting subsequent spontaneous preterm birth. Am J Obstet Gynecol 204(5) 391–e1.

[35]. Graves SW, Esplin MS (2011) 80: Validation of predictive preterm birth biomarkers obtained by maternal serum proteomics. Am J Obstet Gynecol 204(1) S46. [PubMed: 21514920]

[36]. Anfossi L, Di Nardo F, Cavalera S, Giovannoli C, Baggiani C (2018) Multiplex lateral flow immunoassay: An overview of strategies towards high-throughput point-of-need testing. Biosensors 9(1) 2. [PubMed: 30587769]

[37]. Hosseini S, Vázquez-Villegas P, Rito-Palomares M, Martinez-Chapa SO (2018) Advantages, disadvantages and modifications of conventional ELISA. In Enzyme-Linked Immunosorbent Assay (ELISA) (pp. 67–115). Springer Singapore.

[38]. Beauchamp MJ, Nielsen AV, Gong H, Nordin GP, Woolley AT (2019) 3D printed microfluidic devices for microchip electrophoresis of preterm birth biomarkers. Anal Chem 91(11) 7418–7425. [PubMed: 31056901]

[39]. Nielsen AV, Nielsen JB, Sonker M, Knob R, Sahore V, Woolley AT (2018) Microchip electrophoresis separation of a panel of preterm birth biomarkers. Electrophoresis 39(18) 2300–2307. [PubMed: 29683528]

[40]. Almughamsi HM, Howell MK, Parry SR, Esene JE, Nielsen JB, Nordin GP, Woolley AT (2022) Immunoaffinity monoliths for multiplexed extraction of preterm birth biomarkers from human blood serum in 3D printed microfluidic devices. Analyst 147(4) 734–743. [PubMed: 35103723]

[41]. Bickham AV, Pang C, George BQ, Topham DJ, Nielsen JB, Nordin GP, Woolley AT (2020) 3D printed microfluidic devices for solid-phase extraction and on-chip fluorescent labeling of preterm birth risk biomarkers. Anal Chem 92(18) 12322–12329. [PubMed: 32829631]

[42]. Sonker M, Parker EK, Nielsen AV, Sahore V, Woolley AT (2018) Electrokinetically operated microfluidic devices for integrated immunoaffinity monolith extraction and electrophoretic separation of preterm birth biomarkers. Analyst 143(1) 224–231.

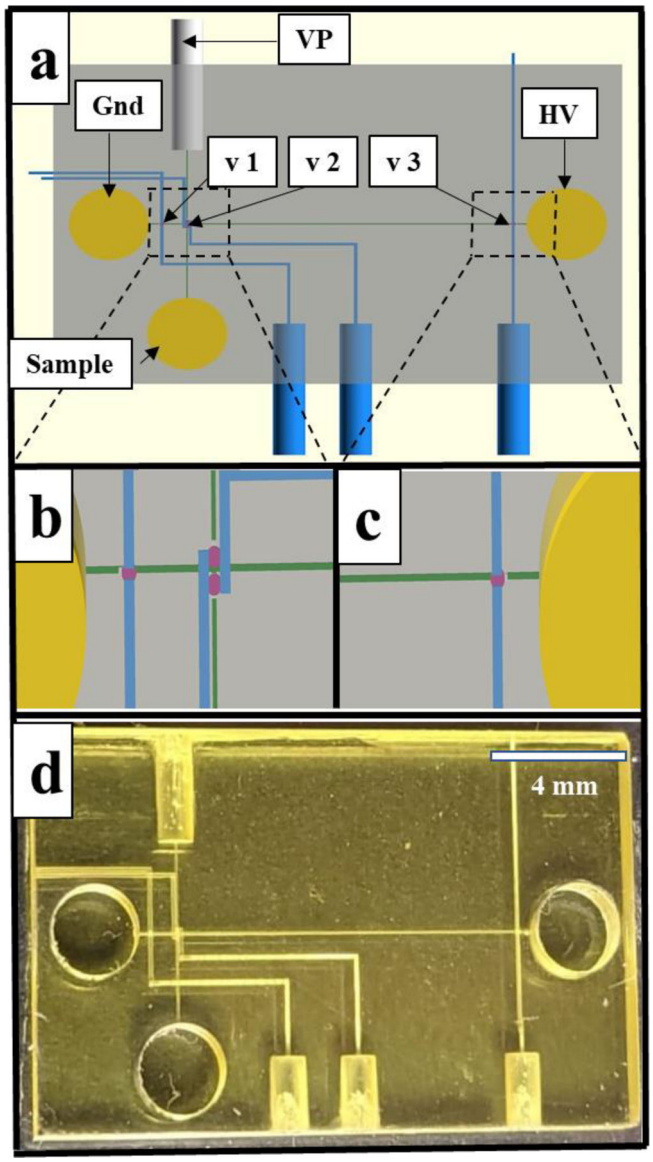

Figure 1.

3D printed, valve integrated devices. (a) OpenSCAD design with channels (green), reservoirs (yellow), valves (purple), and pneumatic lines with connections to the side of the device (blue). Gnd: ground, v: valve, VP: vacuum port, and HV: high voltage. (b–c) Zoom views of SCAD design. (d) Device photograph.

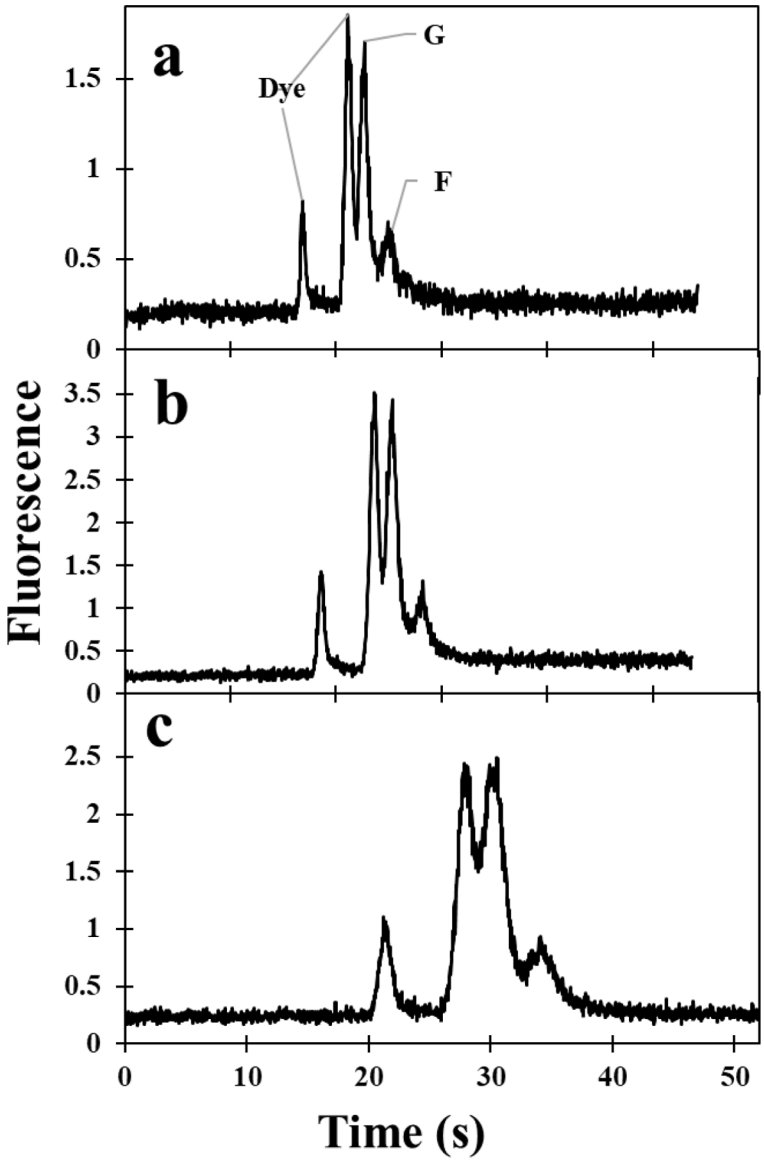

Figure 2.

Microchip electropherograms in 3D printed, valve-injected microfluidic devices. Separation of 80 nM G and 120 nM F in 50 mM HEPES pH 8, with a pressure differential of −7 psi and an injection time of (a) 0.5 s, (b) 1.0 s, and (c) 1.5 s.

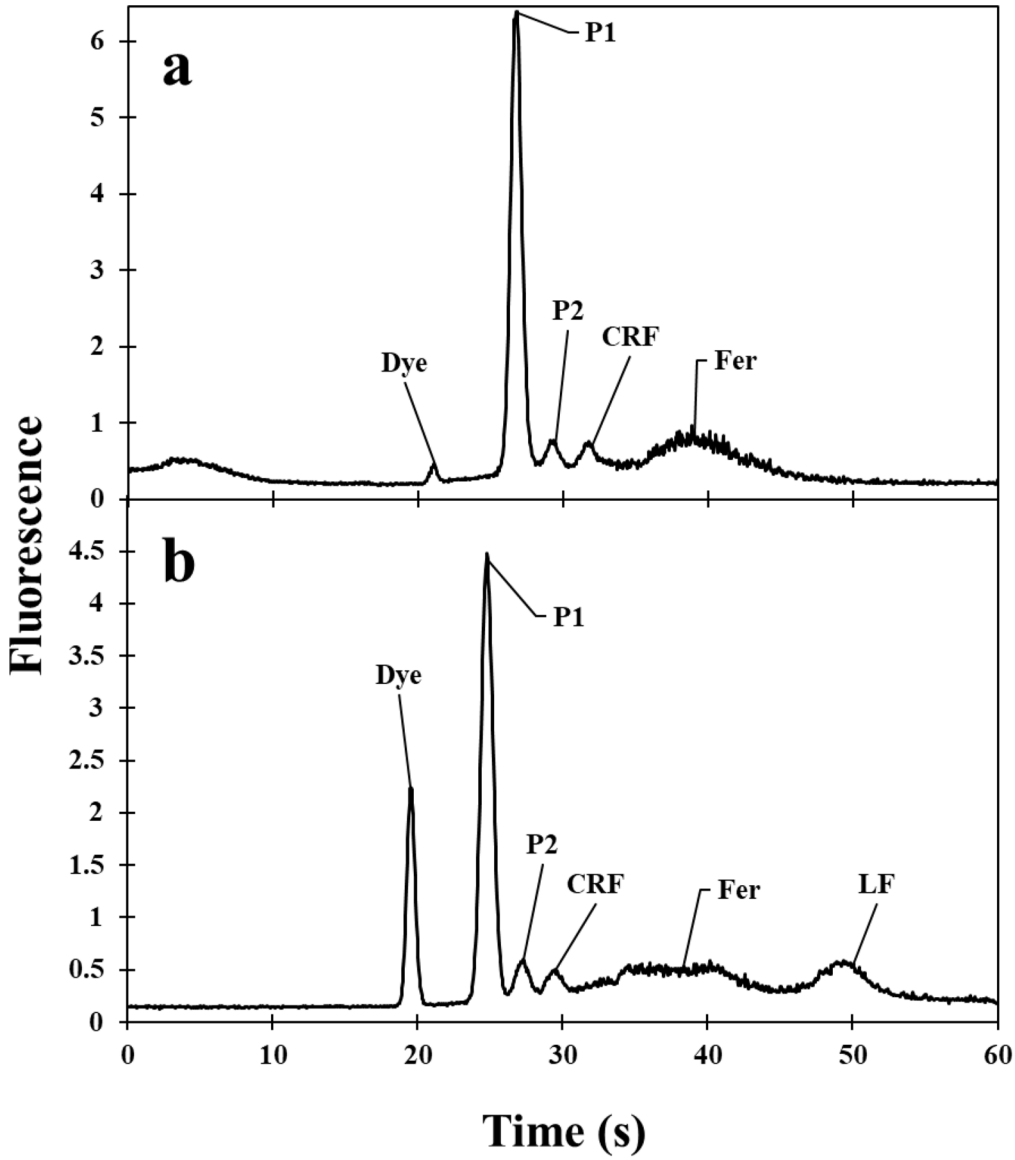

Figure 3.

Microchip electrophoresis of PTB biomarkers. (a) 5 nM P1, 150 nM P2, 15 nM CRF, and 10 nM Fer. (b) 5 nM P1, 200 nM P2, 15 nM CRF, and 10 nM Fer, and 20 nM LF.

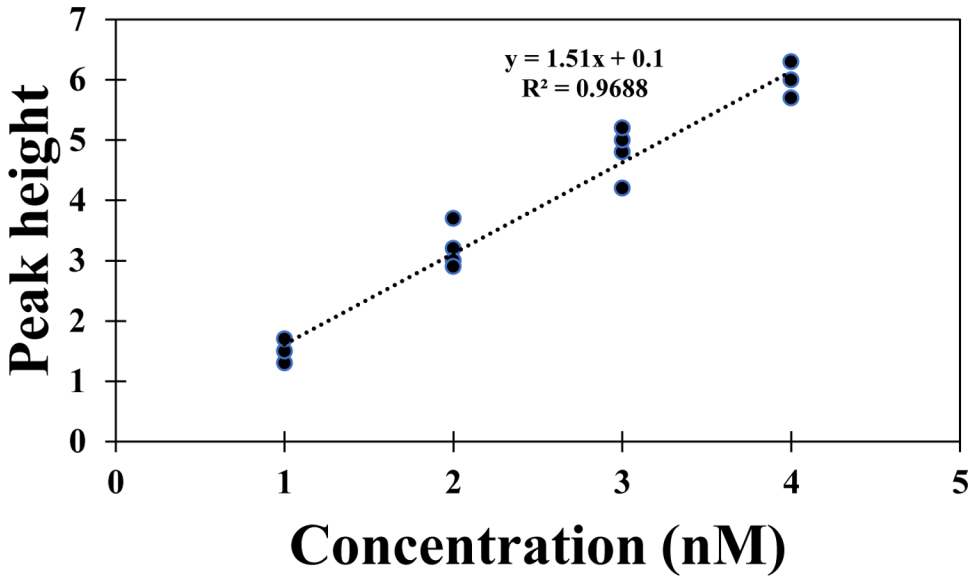

Figure 4.

Calibration plot for determining detection limit for μCE of peptide 1, for an injection time of 1.5 s, in 3D printed microfluidic devices with valves. The LOD is 400 pM.

Table 1.

Comparison of μCE separation performance for different injection times in valve-injected microfluidic devices for three replicate runs. Standard deviations are given in parentheses.

Analyte	Injection time (s)	Height	FWHM	N	Resolution
Glycine	0.5	1.71 (0.21)	0.71 (0.06)	5770 (510)	1.21 (0.18)
	1.0	3.40 (0.45)	1.08 (0.04)	3040 (140)	1.02 (0.14)
	1.5	2.40 (0.53)	1.76 (0.05)	1670 (260)	0.89 (0.11)
Phenylalanine	0.5	0.71 (0.05)	1.10 (0.09)	2850 (620)	
	1.0	1.30 (0.07)	1.39 (0.06)	2310 (250)	
	1.5	0.90 (0.06)	2.10 (0.04)	1480 (220)	

Table 2.

PTB biomarkers separated and the resolution.

Biomarker	Resolution
P1/P2	3.12
P2/CRF	2.80
CRF/Fer	2.31
Fer/LF	1.54

Table 3.

Comparison of methods reported for the analysis of P1 and P2.

Method	Device/ technology	Sample volume (μL)	LOD (nM)	Reference
LC-MS	commercial	50–1000	Not measured	[34]
μCE	3D print	2–10	7 (P1)	[38]
μCE	COC	5–15	3 (P1) 190 (P2)	[39]
μCE	3D print	2–10	0.40 (P1) 15 (P2)	this work